Current Radiology Reports (2024) 12:19–29
https://doi.org/10.1007/s40134-023-00423-2

COMPUTED TOMOGRAPHY (SAVVAS NICOLAOU AND MOHAMMED F. MOHAMMED, SECTION EDITOR)

Diagnostic Role of Dual-Energy Computed Tomography in the Assessment of Musculoskeletal Oncology: A Literature Review

Jumanah Altwalah[1] · Hashim Alsalman[1] · Adnan Sheikh[2]

Accepted: 22 December 2023 / Published online: 12 February 2024

Abstract

Purpose of Review This review aims to consolidate knowledge and recent research findings related to the potential clinical applications of dual-energy computed tomography (DECT) for the identification and characterization of bone lesions. The purpose is to explore the advantages of DECT over traditional imaging techniques in musculoskeletal radiology, particularly in the context of oncologic care for cancer patients.

Recent Findings DECT has emerged as a state-of-the-art imaging technique that offers significant benefits in the detection and assessment of skeletal lesions. It provides improved sensitivity in identifying hidden lesions, including metastatic ones that are often concealed within the marrow space. DECT's advanced technology enables material decomposition and color-coded overlays, allowing for the differentiation of various types of soft tissue mineralization and the evaluation of bone marrow edema and infiltrative skeletal neoplasms. Furthermore, DECT can aid in distinguishing between malignant and benign skeletal lesions, providing valuable diagnostic information for treatment planning and patient care.

Summary Dual-energy computed tomography (DECT) is a promising tool in musculoskeletal radiology, particularly for oncologic care and disease staging in cancer patients. DECT's ability to differentiate, enhance, or suppress various types of tissues through material decomposition and spectral data analysis makes it a valuable imaging technique for identifying and characterizing bone lesions. With its advanced technology, DECT offers improved sensitivity in detecting hidden lesions and provides valuable diagnostic information without increasing radiation exposure. By addressing the limitations of other imaging modalities, DECT has the potential to enhance patient care and improve outcomes in the field of musculoskeletal radiology.

Keywords DECT · Skeletal tumors · Musculoskeletal oncology · CT

Introduction

Dual-energy computed tomography (DECT) has emerged as a state-of-the-art imaging technique in the field of musculoskeletal radiology, offering significant benefits over traditional monoenergetic CT scans. This is particularly important in the context of oncologic care for cancer patients, where accurate disease staging is crucial. While monoenergetic CT imaging can struggle with sensitivity in identifying specific skeletal lesions, especially metastatic ones that tend to be concealed within the marrow space due to the high attenuation of cortical and trabecular bone [1, 2], DECT provides a more advanced solution.

Although magnetic resonance imaging (MRI) is a valuable alternative, it has its limitations, including comparatively longer scan times and unsuitability for claustrophobic patients or those with MRI-incompatible devices. Furthermore, positron emission tomography-computed tomography (PET-CT) is a less accessible option that demands extensive preparation [3]. DECT addresses these challenges and offers a compelling array of advantages, particularly for musculoskeletal imaging. Its cutting-edge technology enables improved sensitivity in detecting hidden lesions, providing valuable insights for disease

✉ Jumanah Altwalah
Jaltwalah@gmail.com

[1] Ministry of National Guard–Health Affairs, Riyadh, Saudi Arabia

[2] Vancouver General Hospital-University of British Columbia, Vancouver, British Columbia, Canada

assessment. DECT's efficiency and accuracy make it a promising tool for enhancing oncologic care and disease staging in cancer patients [4].

DECT has the potential to provide valuable clinical insights using material decomposition, particularly in the field of musculoskeletal imaging. It can be instrumental in various aspects such as evaluating crystal arthropathy, detecting bone marrow edema in suspected occult fractures, identifying periprosthetic fractures, assessing tendon ruptures, reducing metallic artifacts, performing CT arthrography, detecting bone lesions, and aiding in biopsies [3, 5, 6••, 7, 8].

Importantly, this advancement can enhance patient care by delivering improved diagnostic information without increasing radiation exposure [9]. However, it's worth noting that DECT is not commonly utilized for assessing metastatic lesions and infiltrative skeletal neoplasms. This comprehensive review aims to consolidate knowledge and recent research findings related to the potential clinical applications of dual-energy computed tomography (DECT) for the identification and characterization of bone lesions.

Dual-Energy CT Physics and Technology

The physics and technology of dual-energy CT (DECT) are rooted in the intricate interactions between coherent scatter, the Compton effect, and the photoelectric effect, all of which contribute to the radiographic attenuation fundamental to image formation. DECT capitalizes on the distinct behaviors of different materials when exposed to X-rays of varying photon energies, leading to variations in radiographic attenuation and subsequent tissue contrast. To achieve this, DECT employs two X-ray beams operating at different energy levels, typically around 80 and 140 kV, aiming to maximize the differentiation between materials while minimizing spectral overlap in X-ray spectra [4, 10–12, 13•, 14–18].

Materials with higher atomic numbers (Z), like iodine, xenon, and calcium, possess K-edges that closely align with the average energy of the lower kilovoltage photon source. As a result, they tend to absorb more low-energy photons. In contrast, the human body is mainly composed of elements with lower atomic numbers, such as carbon, oxygen, hydrogen, and nitrogen, which have lower K-edge values. Unfortunately, neither the low nor high kilovoltage beams are optimally matched to these values, resulting in roughly equal absorption by these elements. The variations in attenuation between the low and high-energy beams, denoted as the dual-energy index (DEI), serve as the basis for utilizing dual-energy CT to differentiate, enhance, or suppress various types of tissues [4, 10–12, 13•, 14–19].

Hardware Design and Postprocessing Tools

There are four primary methods employed for achieving dual-energy CT imaging. The sequential scanning approach, the earliest dual-energy CT method, involves conducting two separate scans using a single energy source at varying energy levels. Despite its basic hardware requirements, this method entails higher radiation doses and acquisition times, limited capabilities, and intricate post-processing. Currently, the dominant technologies in the market are dual-source (Siemens Healthcare) and rapid kilovoltage switching (GE Healthcare) [4, 18]. The dual-source dual-energy CT scanner employs two X-ray tubes and two detectors oriented perpendicularly in the same gantry to simultaneously capture two datasets with distinct energy levels. The rapid kilovoltage switching method, on the other hand, employs a single tube within a large gantry to swiftly switch energy levels and collect data for each set during a single rotation. Lastly, the double-layer detector technique divides X-ray photons into two energy spectra, with the upper layer absorbing the low-energy spectrum and the lower layer absorbing the higher-energy photo [4, 10, 20–22].

In terms of post-processing, CT images are processed to selectively capture higher-energy photons using image reconstruction algorithms for metallic implants. This process reduces beam hardening and scatter, resulting in a more precise representation of the integrity of the metallic implant [4, 19]. Through a combination of material decomposition and color-coded overlays, gouty tophi can be differentiated from other types of soft tissue mineralization [4, 19, 23]. The generation of virtual noncalcium (VNCa) images is a valuable technique for evaluating bone marrow edema in cases of bone trauma, as well as for assessing infiltrative skeletal neoplasms and metastases [4, 15, 18, 24]. Previous studies focusing on skeletal lesions employed various reconstructions, such as virtual noncalcium (VNCa) images, water hydroxyapatite (water HAP) material decomposition maps, and iodine differentiation maps from contrast-enhanced DECT. VNCa images utilize spectral data to detect calcium, then replacing it with a virtual CT number that approximates the expected CT number without calcium. This approach enhances the definition of bone marrow [6••, 25], aiding in the visualization of skeletal lesions linked to bone marrow edema [26] (Fig. 1). Conversely, water HAP material decomposition maps utilize spectral data of water and hydroxyapatite to identify regions with elevated water concentration while suppressing the bone signal [6••, 27•]. Lastly, contrast-enhanced DECT iodine density mapping quantifies iodine uptake in tissues [28] (Fig. 2).

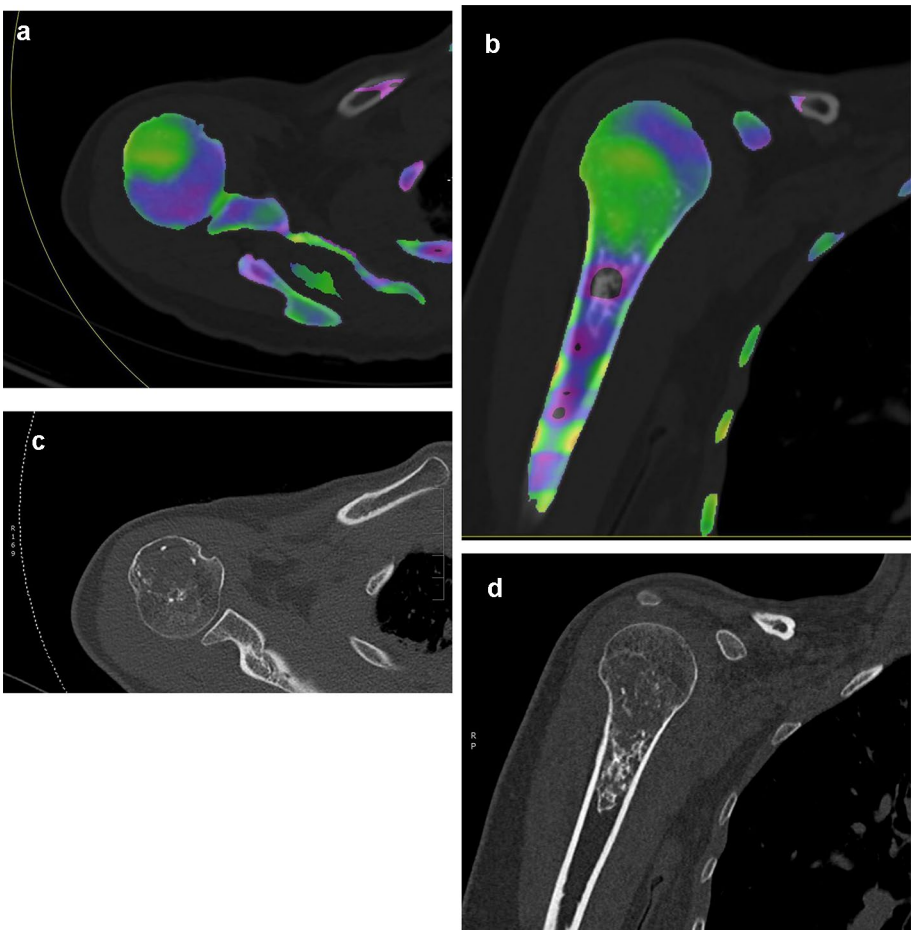

Fig. 1 Non-contrast CT scan of a 43-year-old man with atypical cartilaginous tumor in DECT axial (**a**) and coronal (**b**) VNCa images demonstrating increased attenuation (color-coded as green) in the proximal humerus that correlates with the lytic lesion which chondroid matrix seen in axial bone window (**c**) and coronal (**d**) (Color figure online)

Differentiating Malignant Neoplasms from Other Benign Lesions

Distinguishing between malignant and benign skeletal lesions can be a complex task. The challenge is particularly evident when attempting to differentiate osteoblastic metastatic lesions from bone islands (enostoses), as their appearances on monoenergetic CT scans can be quite similar, both exhibiting hyperdense focal characteristics. To aid in distinguishing them, attenuation differences play a crucial role. Specifically, for identifying osteoblastic metastasis, an attenuation measurement lower than 885 Hounsfield Units on a standard computed tomography scan is indicative of a preferred pathological abnormality [29].

In a retrospective study by Yue Dong et al., involving 94 patients with osteoblastic pulmonary metastases, DECT material decomposition using water was employed to characterize these lesions. This approach revealed that osteoblastic metastases displayed reduced bone densities, whereas bone islands exhibited heightened densities. Additionally, the spectral curve slope for osteoblastic metastasis was more distinct. This distinction can be attributed to the fact that osteoblastic metastasis replaces and damages the original bone, leading to decreased density and increased water content. Conversely, a bone island constitutes normal cortical bone within the vertebral body's medullary cavity, thus displaying higher bone density but lower water content compared to osteoblastic metastasis [30].

Schmorl's nodes represent a condition where the nucleus pulposus extends through the vertebral endplate, resulting in gradual bone compression without significant reduction in bone content [31]. These nodes can manifest as focal low-density vertebral lesions, which may mimic osteolytic metastasis. Research has shown that osteolytic metastasis exhibits elevated vascularity compared to normal tissue, leading to increased water content and decreased bone content [32]. Zheng et al. discovered that both metastatic lesions and Schmorl's nodes displayed lower bone densities and higher water densities when compared to normal vertebrae. Importantly, they found that water density was higher in metastatic lesions than in Schmorl's nodes, and the average bone density of metastatic lesions was lower than that of Schmorl's nodes [31].

Furthermore, the spectral characteristics of metastatic lesions and Schmorl's nodes exhibited differences. The most effective differentiation method involved assessing

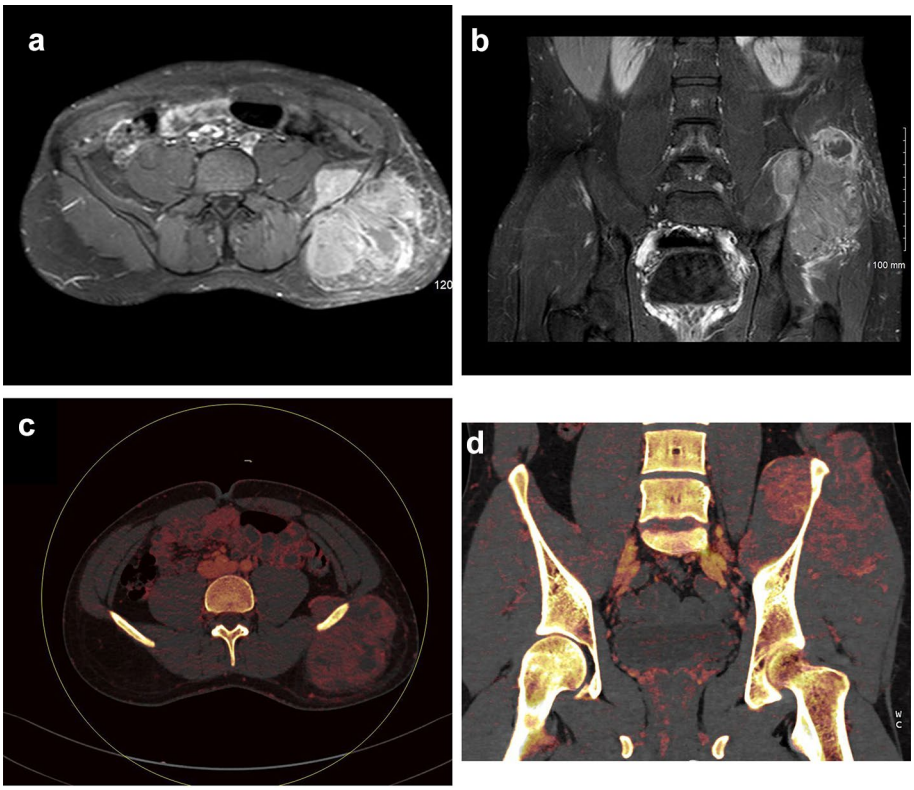

Fig. 2 A gadolinium-enhanced MRI scan of a 16-year-old male with Ewing sarcoma in **a** axial and **b** coronal showed avidly enhancing soft tissue tumor arising from the left iliac crest, an area of necrosis is seen at the superior aspect of the tumor. The **c** axial and **d** coronal DECT VNCa iodine overlay map show comparable avid enhancement with areas of necrosis

Hounsfield Unit values on virtual monoenergetic images at a lower energy range. Here, the mean HU of Schmorl's nodes was higher than that of metastatic lytic lesions. Through DECT, osteolytic spinal metastases can be differentiated from Schmorl's nodes with a sensitivity of 90% and specificity of 88% [31].

Skeletal Metastasis

Advanced stages of cancer often correlate with unfavorable prognoses and bone metastases [28, 32–34]. Detecting these lesions is crucial for tailoring treatments and preventing potential skeletal complications like severe pain and fractures [35, 36]. Despite contrast-enhanced computed tomography (CT) being a routine tool for cancer staging and follow-up, its sensitivity in detecting bone metastases is limited. Different forms of osseous metastasis, including osteolytic, osteoblastic, mixed, or confined within the bone marrow, exist [27, 35–37]. Around 33% of osseous metastases account for bone marrow lesions [38–40]. Identifying metastatic lesions that do not cause bone destruction or osteoblastic changes using conventional CT imaging is challenging. Dual-energy CT (DECT) could play a role in assessing skeletal metastasis (Fig. 3).

In DECT, osteolytic metastases are discerned by reduced bone content, marrow replacement, and increased water content due to heightened vascular permeability. DECT offers three potential methods to aid in assessing metastasis from benign lesions. These include quantitative tissue decomposition using spectral curve and slope patterns, qualitative tissue decomposition such as VNCa bone marrow color maps, and iodine mapping to quantify iodine uptake as a marker of vascularity [4].

Virtual noncalcium (VNCa) imaging enhances the visualization of neoplastic marrow infiltration by showing altered colors or higher Hounsfield Unit (HU) values through qualitative tissue decomposition. This technique improves the detection of subtle metastases [4, 41, 42]. The use of color-coded bone marrow images increases sensitivity, specificity, positive predictive value, negative predictive value, and accuracy in identifying lytic and blastic bone metastases. A study by Ghada Issa et al. improved sensitivity in detecting skeletal metastasis from 78.2% with conventional CT to 89.8% using DECT [43].

Some limitations have been observed while using virtual noncalcium imaging to assess bone marrow edema. The masking effect of the bone cortex can cause the subtraction of high-attenuation pixels and lead to inaccuracies when assessing bone marrow edema close to the cortical bone [44]. Moreover, artifacts are noticeable when there are substantial sclerosis and gas locules, which restrict the assessment of vertebral bodies with a height of less than 4 mm [15].

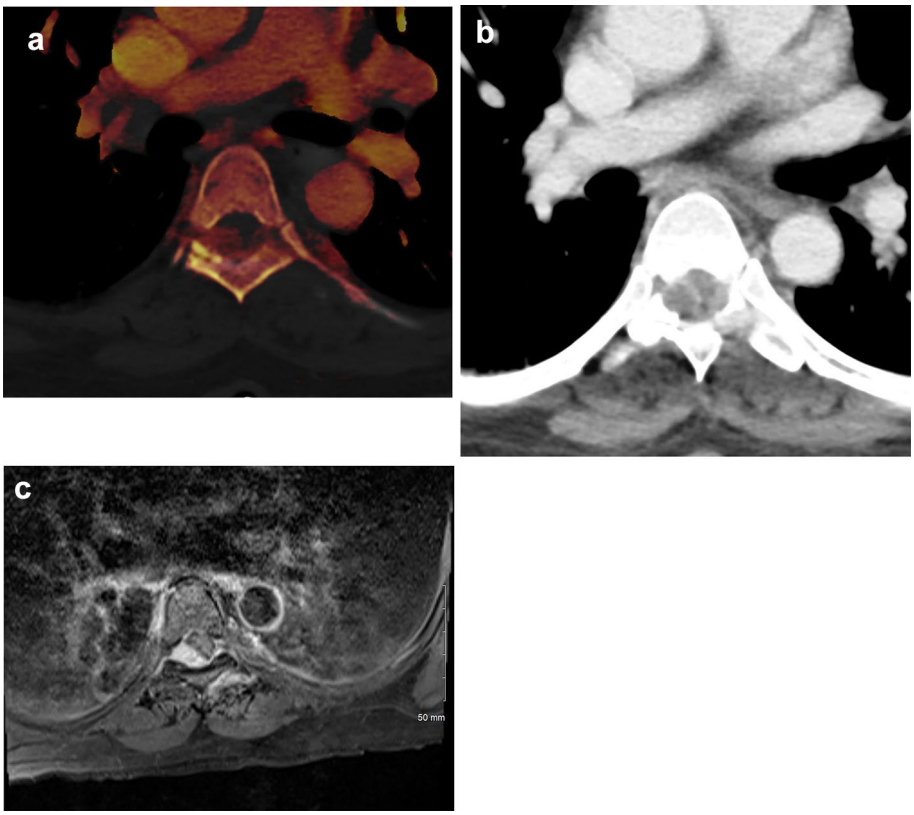

Fig. 3 Contrast-enhanced CT scan of a 56-year-old woman with metastatic breast cancer in axial **a** VNCa iodine overlay map shows intracanal lesion with avid enhancement on the and involves the left lamina in **b** soft tissue window the intracanal lesion is not clearly visible. **c** Axial gadolinium-enhanced MRI confirms the metastatic lesion as seen on the CT scan

Detecting edema becomes challenging with degenerative changes or suboptimal parameter settings. Additionally, the algorithm can't differentiate between edema, neoplasm, or red marrow, sometimes leading to false positives in color maps [45]. Detection is most effective in predominantly yellow marrow backgrounds [46]. Inter-reader variability can occur due to the learning curve associated with dual-energy CT images [47].

Lower energy 40 keV virtual monoenergetic imaging is found to differentiate metastasis and osteolytic lesions better due to high-water content and lower bone attenuation in metastasis, as well as the downward slope of the spectral curve in metastatic lesions [31, 42]. Contrast-enhanced studies using iodine maps can evaluate vascularity of soft tissue components in osteolytic lesions and indicate malignancy when significant iodine uptake is present [42].

Prompt detection of pathologic fractures is essential, as they result from metastasis and infiltrative skeletal lesions, leading to pain, morbidity, and reduced survival rates [33, 34]. Distinguishing between fracture hematoma and subtle infiltrative lesions is challenging with conventional CT. DECT can help detect underlying malignant pathology (Fig. 4). In a small retrospective study, DECT bone marrow maps differentiated 15 pathological fractures from non-pathological fractures based on HU attenuation values. Pathologic fractures had higher values, not evident in monoenergetic CT images [48]. Establishing a definitive HU threshold on virtual non-contrast attenuation (VNCa) image maps requires more extensive studies with larger sample sizes.

Multiple Myeloma

Multiple myeloma (MM) stands as one of the prevalent hematological malignancies, with approximately 90% of MM patients presenting osseous lesions [49]. Whole-body low-dose CT remains a common screening method for myeloma and is recommended as the primary imaging technique for assessing bone lesions in newly diagnosed patients [50–52]. Nonetheless, non-osteolytic lesions, often obscured by dense trabecular bone, pose a visualization challenge on single-energy CT. As a result, MRI or FDG PET is typically employed to investigate these lesions [53]. Recently, several studies have explored the utility of DECT for diagnosing, screening, and assessing the response of MM lesions (Fig. 5).

Kosmala et al. conducted a pioneering study that evaluated DECT's sensitivity and specificity using virtual non-calcium (VNCa) images in detecting non-osteolytic bone marrow (BM) infiltration in multiple myeloma patients, comparing the results with MRI. Their small prospective study demonstrated DECT's overall sensitivity of 91.3% and specificity of 90.9% in detecting non-osteolytic BM lesions. They further examined Hounsfield unit (HU)

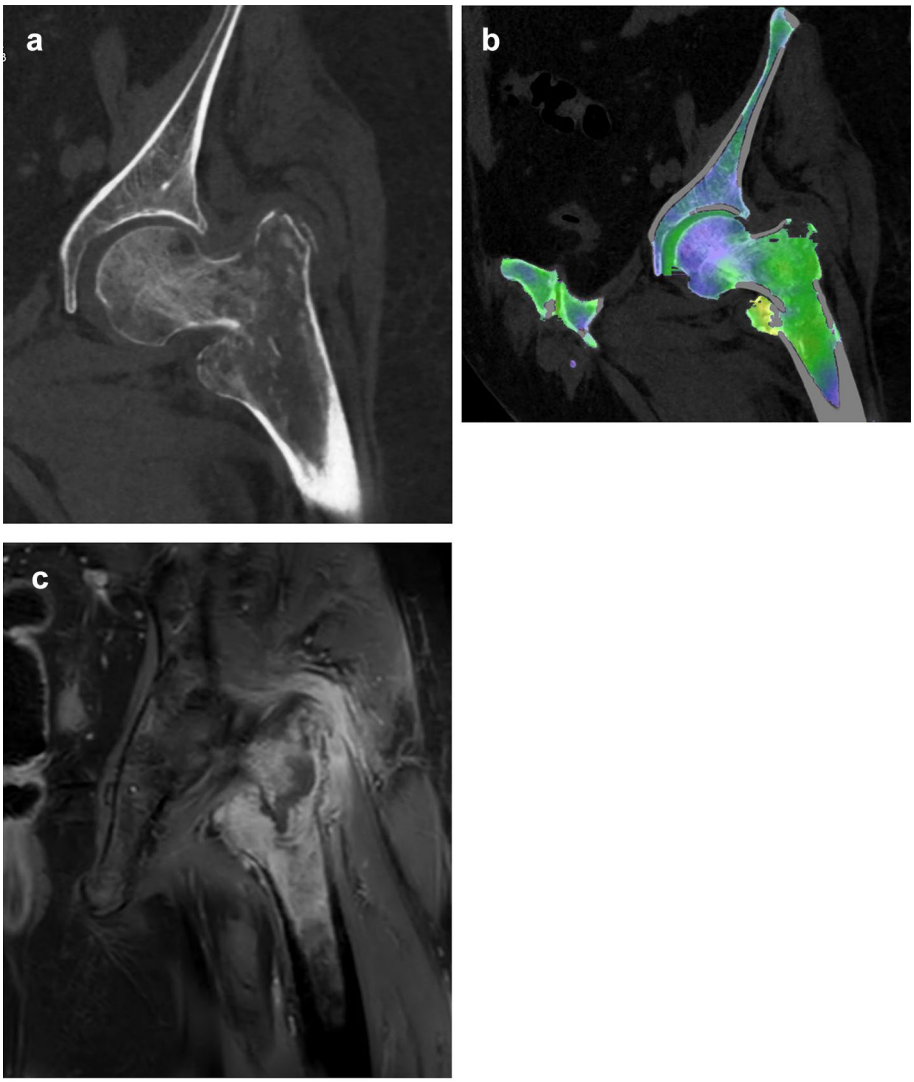

Fig. 4 Non-contrast CT scan coronal images of a 60-year-old man who presented to the emergency with a history of fall. Coronal images in **a** bone window and **b** VNCa images show intertrochanteric fracture with underlying ill-defined lucency of the proximal femur increased attenuation (color-coded as green) in the proximal femur represents an underlying lesion that correlates with enhancing tumor on coronal gadolinium MRI scan in coronal image **c**. The underlying lesion was pathology proven to be lymphoma (Color figure online)

attenuation values of the lesions, revealing that a cut-off of − 44.9 HU provided sensitivity of 93.3%, specificity of 92.4%, and accuracy of 92.7% in detecting BM infiltration. The DECT VNCa technique proves to be a reliable method for identifying and diagnosing bone marrow infiltration in individuals with myeloma [54].

DECT attenuation values on VNCa images can offer further characterization of skeletal lesions in MM patients. A prospective study assessed DECT attenuation values on VNCa images across the entire skeleton, correlating calcium-subtracted attenuation with the degree of bone marrow infiltration by plasma cells. In a group of 21 consecutive MM patients, a positive correlation emerged between the attenuation value and the level of bone marrow infiltration, with a median average attenuation of − 59.9 HU. This finding holds potential for enabling earlier MM detection through an objective measurement of marrow involvement [55].

Another retrospective study investigated HU attenuation values of bone marrow on VNCa images, differentiating between normal, focal, and diffuse imaging patterns in 53 subjects. An attenuation value cut-off of − 35.7 HU demonstrated 100% sensitivity and 97% specificity in identifying diffuse patterns compared to normal patterns. Similarly, a cut-off of − 31.9 HU could distinguish focal from normal patterns with 97% sensitivity and 99% specificity [56].

The disease activity of multiple myeloma correlated with the attenuation value of bone lesions on DECT VNCa imaging. Active disease exhibited a mean Hounsfield unit of 12.4 HU, whereas inactive disease had − 25.3 HU (SD, 32.0) ($p < 0.001$). Moreover, a negative correlation was established between the T1 signal intensity of osseous lesions on MRI and the attenuation on VNCa images. Distinguishing active and non-active lesions was possible at a cut-off value of − 21.4 HU, yielding 92% sensitivity and 58% specificity [57]. The response of MM lytic bone lesions (LBL) to

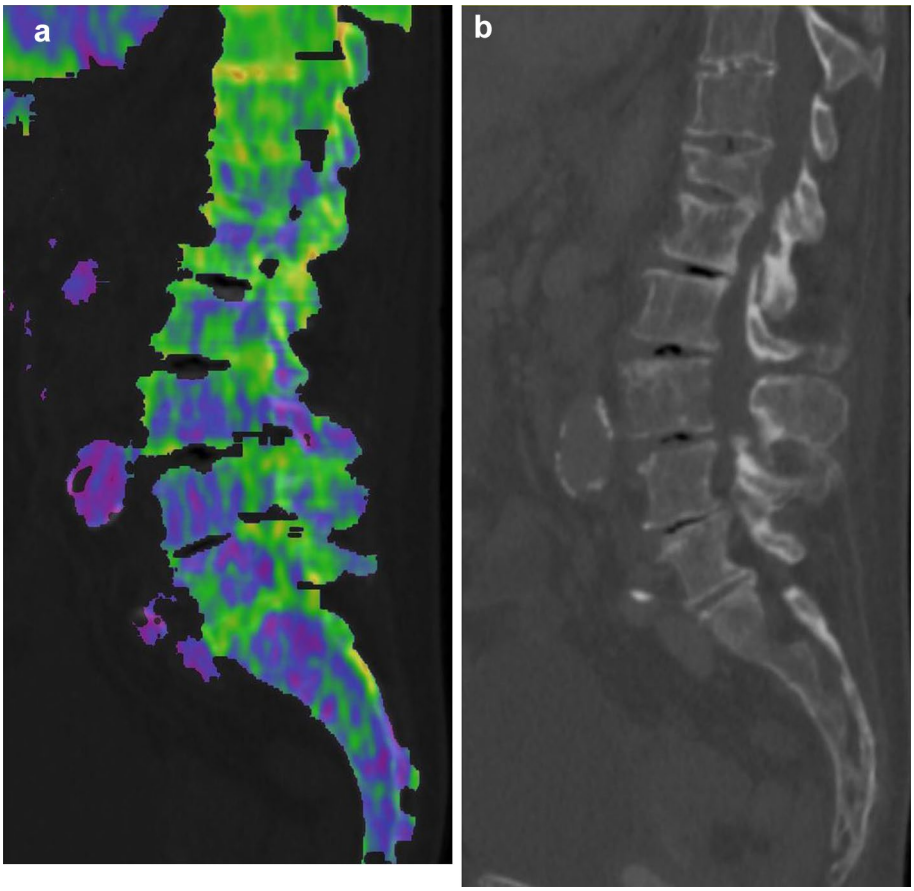

Fig. 5 Sagittal color-coded dual-energy CT images **a** show bone marrow lesions (green); these marrow infiltrations do not correlate with lytic lesions on bone window **b** images. Artificial overlay of the spinal canal and the aorta results from the automatic post-processing software (Color figure online)

radiation was assessed in a study, demonstrating decreased attenuation values of irradiated lesions compared to non-irradiated control lesions from the same patients. The attenuation of LBL typically diminished over time post-irradiation, with an identified absolute threshold for detection after 2000 days of − 77.0 to − 22.5 HU on VNCa images [58].

The variations in mean Hounsfield values across these studies stem from differences in technology, software, and scanning protocols. Manufacturers' differences in acquiring and processing spectral data on various scanners account for variations in HU values. Challenges in comparing and applying dual-energy CT protocols impede validation for clinical use. Material decomposition algorithms need re-establishment with each scanner generation, which could hinder progress.

Soft Tissue Lesions

The enhanced capabilities of dual-energy computed tomography (DECT) in detecting and characterizing tumors have been widely acknowledged in the genitourinary, gastroenterology, and pulmonary fields [59–62].

While our literature review did not yield specific research assessing DECT in soft tissue tumors of the musculoskeletal system, it's reasonable to infer that the same principles that apply to other body regions can be extrapolated. Numerous DECT applications contribute to the diagnosis and monitoring of soft tissue tumors.

The virtual non-contrast (VNC) application has emerged as a valuable tool, enhancing the evaluation of tumor enhancement and vascularity by enabling material decomposition and producing iodine map images. By accurately quantifying iodine concentration within the lesion, the iodine level corresponds to perfused blood volume and vascularity, indicative of angiogenesis and malignancy. This application boosts lesion detection by amplifying the attenuation discrepancy between the lesion and surrounding normal tissues [59, 63–65].

Assessing iodine concentration in the VNC application also offers insight into treatment response and tumor viability, effectively serving as a biomarker [26, 66].

Additionally, the VNC application facilitates iodine subtraction, generating a virtual non-contrast study. This eliminates the need for a pre-contrast scan, thereby reducing radiation exposure [9, 67].

In the context of vascular tumors, analyzing enhancement patterns on iodine map images proves invaluable for diagnosis, offering a more comprehensive view of iodine distribution compared to standard conventional CT scans [68–70]. Furthermore, the vascular application of DECT enhances the clarity of vascular supply delineation by eliminating osseous structures from the scanned image. Through dual-energy techniques, the differentiation between iodine and adjacent bone can be achieved in a single acquisition, followed by a straightforward post-processing step with accurate outcomes [71] (Fig. 6).

Metal Artifacts Reduction

Metallic prostheses often introduce image artifacts, which in turn hinder the accurate assessment of surrounding structures. Dual-energy computed tomography (DECT) offers a solution by enabling the acquisition of virtual monoenergetic images. These images simulate the output of a monochromatic X-ray beam, mitigating beam hardening artifacts and enhancing overall image quality. Virtual monoenergetic images prove especially beneficial in the presence of metallic prostheses, improving diagnostic accuracy [72].

Numerous studies have established that the most effective reduction in metallic artifacts occurs with high-energy reconstructed images, typically ranging between 105 and 133 kV. However, it's important to note that the extent of metallic artifact reduction can vary based on the type and size of the prosthesis [73–75].

A phantom study evaluating various metal artifact reduction techniques for tumor delineation found that DECT 130 KeV virtual monoenergetic images exhibited the most significant enhancement in representing Hounsfield Unit (HU) attenuation of spine implant phantoms, improving from 35 to 79%. Furthermore, these images demonstrated the most accurate contours [76]. Other investigations have revealed that monoenergetic images, in some instances, exclusively visualized periprosthetic lesions that were not apparent on single-energy CT scans [73, 74].

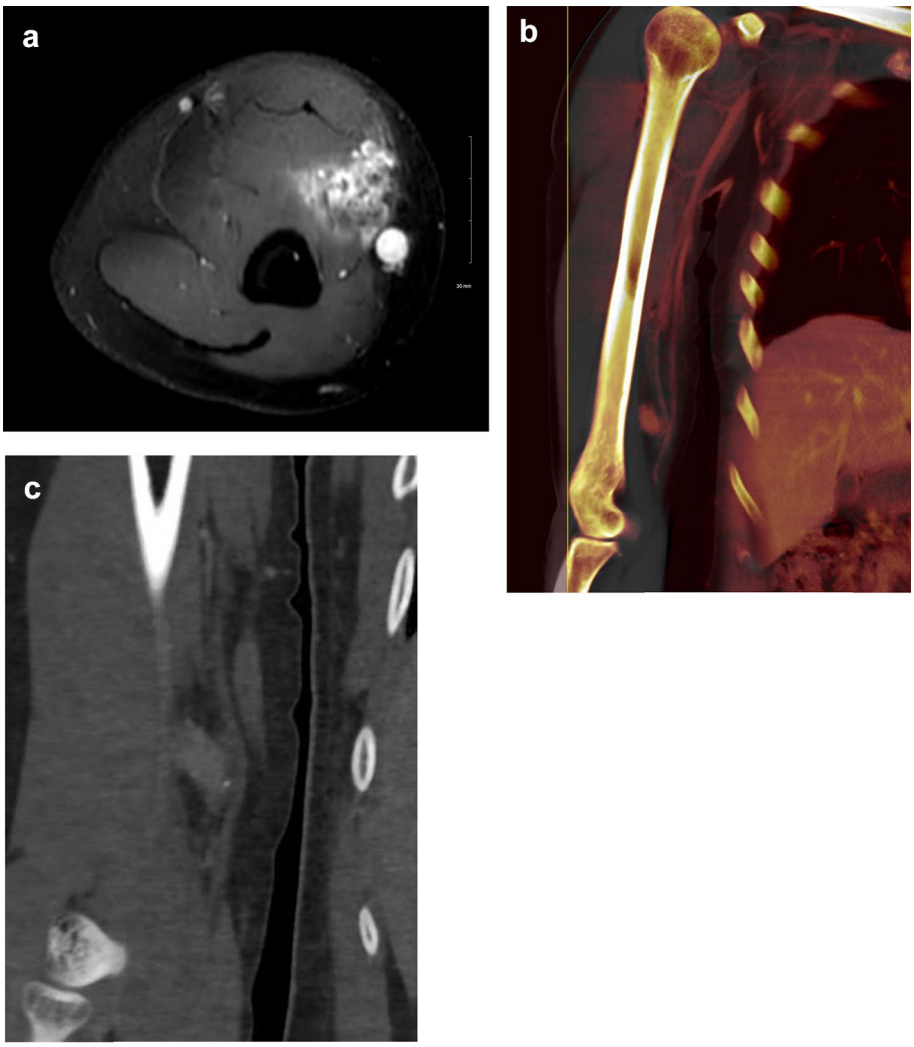

Fig. 6 Gadolinium-enhanced MRI scan of a 21-year-old female with soft tissue hemangioma in axial image **a** demonstrates a heterogenous enhancing soft tissue lesion in the distal arm. Contrast-enhanced CT scan in **b** oronal iodine overlay map image delineates the vascular supply of the lesion and **c** coronal virtual non-contrast image shows small phlebolith in the inferior aspect of the lesion

Despite the benefits of virtual monoenergetic images in reducing beam hardening artifacts, challenges such as photon starvation artifacts can still arise, especially with larger metallic prostheses. To address this, a metal artifact reduction (MAR) algorithm utilizes metal segmentation to diminish severe artifactual streaks in the image. However, it's worth noting that while MAR can alleviate artifacts, it might introduce new artifacts in the form of bright and dark streaks [77–79] and it may slightly underestimate prosthesis size [80–83]. Radiologists should exercise caution and obtain both MAR-applied and non-MAR images to prevent misinterpretation. Creating multiplanar reconstructed images can further enhance the accuracy of assessment.

Conclusion

In conclusion, dual-energy computed tomography (DECT) is a valuable imaging technique in musculoskeletal radiology. It offers enhanced sensitivity in detecting and characterizing bone lesions, particularly metastatic ones. DECT overcomes limitations of other imaging modalities and provides accurate diagnostic information without increasing radiation exposure. By differentiating malignant and benign lesions, DECT helps in disease assessment and staging. Overall, DECT has the potential to significantly improve patient care and oncologic management.

Author Contributions All authors contributed in writing the main manuscript text and prepared figures. All authors reviewed the manuscript.

Funding Not applicable.

Data Availability Not applicable.

Declarations

Competing Interests The authors have no competing interests as defined by Springer, or other interests that might be perceived to influence the results and/or discussion reported in this paper.

Ethical Approval Not applicable

Research Involving Human and Animal Rights This article does not contain any studies with human or animal subjects performed by any of the authors.

References

Papers of particular interest, published recently, have been highlighted as:

- • Of importance
- •• Of major importance

1. Yang P, Wu G, Chang X. Diagnostic accuracy of dual-energy computed tomography in bone marrow edema with vertebral compression fractures: a meta-analysis. Eur J Radiol. 2017;99:124–9.
2. Heindel W, Gübitz R, Vieth V, Weckesser M, Schober O, Schäfers M. The diagnostic imaging of bone metastases. Dtsch Ärztebl Int. 2014. https://doi.org/10.3238/arztebl.2014.0741.
3. Chen H, Zhang Y, Pang J, Wu Z, Jia M, Dong Q, et al. The differentiation of soft tissue infiltration and surrounding edema in an animal model of malignant bone tumor: evaluation by dual-energy CT. Technol Cancer Res Treat. 2019;18:153303381984684.
4. Mallinson PI, Coupal TM, McLaughlin PD, Nicolaou S, Munk PL, Ouellette HA. Dual-energy CT for the musculoskeletal system. Radiology. 2016;281(3):690–707.
5. Yang HL, Liu T, Wang XM, Xu Y, Deng SM. Diagnosis of bone metastases: a meta-analysis comparing 18FDG PET, CT MRI and bone scintigraphy. Eur Radiol. 2011;21(12):2604–17.
6. ••Tan M, Lloyd TB. Utility of dual energy computed tomography in the evaluation of infiltrative skeletal lesions and metastasis: a literature review. Skeletal Radiol. 2022;51:1731–41. (This recent article discusses the advanced usage of DECT in skeletal tumors.)
7. Burke MC, Garg A, Youngner JM, Deshmukh S, Omar IM. Initial experience with dual-energy computed tomography-guided bone biopsies of bone lesions that are occult on monoenergetic CT. Skeletal Radiol. 2019;48:605–13.
8. Omoumi P, Rubini A, Dubuc JE, Vande Berg BC, Lecouvet FE. Diagnostic performance of CT-arthrography and 1.5T MR-arthrography for the assessment of glenohumeral joint cartilage: a comparative study with arthroscopic correlation. Eur Radiol. 2015;25(4):961–9.
9. Jiang XY, Zhang SH, Xie QZ, et al. Evaluation of virtual noncontrast images obtained from dual-energy CTA for diagnosing subarachnoid hemorrhage. AJNR Am J Neuroradiol. 2015;198:840–5.
10. Johnson TRC. Dual-energy CT: general principles. Am J Roentgenol. 2012;199(5_supplement):S3-8.
11. Katsura M, Sato J, Akahane M, Kunimatsu A, Abe O. Current and novel techniques for metal artifact reduction at CT: practical guide for radiologists. RadioGraphics. 2018;38(2):450–61.
12. Albrecht MH, Vogl TJ, Martin SS, Nance JW, Duguay TM, Wichmann JL, et al. Review of clinical applications for virtual monoenergetic dual-energy CT. Radiology. 2019;293(2):260–71.
13. •Koch V, Yel I, Grünewald L, Beckers S, Burck I, Lenga L, et al. Assessment of thoracic disk herniation by using virtual noncalcium dual-energy CT in comparison with standard grayscale CT. Eur Radiol. 2021;31:9221–31. (This article assesses disc herniation on DECT which is a common finding and can be misdiagnosed with a skeletal lesion.)
14. Otrakji A, Digumarthy SR, Lo Gullo R, Flores EJ, Shepard JAO, Kalra MK. Dual-energy CT: spectrum of thoracic abnormalities. RadioGraphics. 2016;36(1):38–52.
15. Wang CK, Tsai JM, Chuang MT, Wang MT, Huang KY, Lin RM. Bone marrow edema in vertebral compression fractures: detection with dual-energy CT. Radiology. 2013;269:525–33.
16. Siegel MJ, Ramirez-Giraldo JC. Dual-energy CT in children: imaging algorithms and clinical applications. Radiology. 2019;291(2):286–97.
17. Kaza RK, Platt JF, Cohan RH, Caoili EM, Al-Hawary MM, Wasnik A. Dual-energy CT with single- and dual-source scanners: current applications in evaluating the genitourinary tract. RadioGraphics. 2012;32(2):353–69.
18. Petritsch B, Kosmala A, Weng A, Krauss B, Heidemeier A, Wagner R, et al. Vertebral compression fractures: third-generation dual-energy CT for detection of bone marrow edema at visual and quantitative analyses. Radiology. 2017;284(1):161–8.
19. Dwijendra S, Burke M. Application of dual-energy computed tomography in bone lesion biopsy. Adv Clin Radiol. 2020;2:273–84.

20. McCollough CH, Leng S, Yu L, Fletcher JG. Dual- and multi-energy CT: principles, technical approaches, and clinical applications. Radiology. 2015;276(3):637–53.
21. Yoshizumi T. Dual energy CT in clinical practice. Med Phys. 2011;38(11):6346–6346.
22. Glazebrook KN, Guimarães LS, Murthy NS, Black DF, Bongartz T, Manek N, et al. Identification of intraarticular and periarticular uric acid crystals with dual-energy CT: initial evaluation. Radiology. 2011;261(2):516–24.
23. Wortman JR, Uyeda JW, Fulwadhva UP, Sodickson AD. Dual-energy CT for abdominal and pelvic trauma. RadioGraphics. 2018;38(2):586–602.
24. Abdullayev N, Hokamp NG, Lennartz S, Holz J, Romman Z, Pahn G, et al. Improvements of diagnostic accuracy and visualization of vertebral metastasis using multi-level virtual non-calcium reconstructions from dual-layer spectral detector computed tomography. Eur Radiol. 2019;29:1–9.
25. Palmer W, Simeone F. Can dual-energy CT challenge MR imaging in the diagnosis of focal infiltrative bone marrow lesions? Radiology. 2018;286(1):214–6.
26. Chong CCW, Rai S, Nicolaou S. Dual energy CT in musculoskeletal tumors. In: De Cecco CN, Laghi A, Schoepf UJ, Meinel FG, editors. Dual energy CT in oncology. Cham: Springer; 2015. p. 123–54.
27. •Ishiwata Y, Hieda Y, Kaki S, Aso S, Horie K, Kobayashi Y, et al. Improved diagnostic accuracy of bone metastasis detection by water-HAP associated to non-contrast CT. Diagnostics. 2020;10:853. (This article discusses the advantages of DECT water-HAP images alongside plain CT scans to enhance the diagnostic accuracy of initial staging.)
28. Borggrefe J, Neuhaus V, Blanc ML, Hokamp NG, Maus V, Mpotsaris A, et al. Accuracy of iodine density thresholds for the separation of vertebral bone metastases from healthy-appearing trabecular bone in spectral detector computed tomography. Eur Radiol. 2018;29:3253–61.
29. Ulano A, Bredella MA, Burke P, Chebib I, Simeone FJ, Huang AJ, Torriani M, Chang CY. Distinguishing untreated osteoblastic metastases from enostoses using CT attenuation measurements. AJR. 2016;207(2):362–8. https://doi.org/10.2214/AJR.15.15559.
30. Dong Y, Zheng S, Machida H, Wang B, Liu A, Liu Y, et al. Differential diagnosis of osteoblastic metastases from bone islands in patients with lung cancer by single-source dual-energy CT: advantages of spectral CT imaging. Eur J Radiol. 2015;84(5):901–7.
31. Zheng S, Dong Y, Miao Y, Liu A, Zhang X, Wang B, et al. Differentiation of osteolytic metastases and Schmorl's nodes in cancer patients using dual-energy CT: advantage of spectral CT imaging. Eur J Radiol. 2014;83(7):1216–21.
32. Jain RK. Determinants of tumor blood flow: a review. Cancer Res. 1988;48(10):2641–58.
33. Guillevin R, Vallee JN, Lafitte F, Menuel C, Duverneuil NM, Chiras J. Spine metastasis imaging: review of the literature. J Neuroradiol. 2007;34(5):311–21.
34. David RG. Mechanisms of bone metastasis. N Engl J Med. 2004;350(16):1655–64.
35. Horger M, Thaiss WM, Wiesinger B, Ditt H, Fritz J, Nikolaou K, et al. Longitudinal computed tomography monitoring of pelvic bones in patients with breast cancer using automated bone subtraction software. Invest Radiol. 2017;52(2):288–94.
36. Mundy GR. Metastasis to bone: causes, consequences and therapeutic opportunities. Nat Rev Cancer. 2002;2(8):584–93.
37. Gdowski A, Ranjan AP, Vishwanatha JK. Current concepts in bone metastasis, contemporary therapeutic strategies and ongoing clinical trials. J Exp Clin Cancer Res. 2017. https://doi.org/10.1186/s13046-017-0578-1.
38. Yamaguchi T, Tamai K, Yamato M, Honma K, Ueda Y, Saotome K. Intertrabecular pattern of tumors metastatic to bone. Cancer. 1996;78(7):1388–94.
39. Suzuki A, Kashiwagi N, Doi H, Ishii K, Doi K, Kitano M, Kozuka T, Hyodo T, Tsurusaki M, Yagyu Y, Nakanishi K. Patterns of bone metastases from head and neck squamous cell carcinoma. Auris Nasus Larynx. 2020;47(2):262–7.
40. Ahmed F, Muzaffar R, Fernandes H, Tu Y, Albalooshi B, Osman MM. Skeletal metastasis as detected by 18F-FDG PET with negative CT of the PET/CT: frequency and impact on cancer staging and/or management. Front Oncol. 2016. https://doi.org/10.3389/fonc.2016.00208/full.
41. Rajiah P, Sundaram M, Subhas N. Dual-energy CT in musculoskeletal imaging: what is the role beyond gout? Am J Roentgenol. 2019;213(3):493–505.
42. Kraus M, Weiss J, Selo N, Flohr T, Notohamiprodjo M, Bamberg F, et al. Spinal dual-energy computed tomography: improved visualisation of spinal tumorous growth with a noise-optimised advanced monoenergetic post-processing algorithm. Neuroradiology. 2016;58(11):1093–102.
43. Issa G, Davis DL, Mulligan ME. The ability of dual-energy computed tomography to distinguish normal bone marrow from metastases using bone marrow color maps. J Comput Assist Tomogr. 2018;42:552–8.
44. Pache G, Krauss B, Strohm PC, Saueressig U, Blanke P, Bulla S, et al. Dual-energy CT virtual noncalcium technique: detecting posttraumatic bone marrow lesions–feasibility study. Radiology. 2010;256:617–24.
45. Reddy T, McLaughlin PD, Mallinson PI, Reagan AC, Munk PL, Nicolaou S, et al. Detection of occult, undisplaced hip fractures with a dual-energy CT algorithm targeted to detection of bone marrow edema. Emerg Radiol. 2015;22(1):25–9.
46. Kaup M, Wichmann JL, Scholtz JE, Beeres M, Kromen W, Albrecht MH, et al. Dual-energy CT–based display of bone marrow edema in osteoporotic vertebral compression fractures: impact on diagnostic accuracy of radiologists with varying levels of experience in correlation to MR imaging. Radiology. 2016;280(2):510–9.
47. Guggenberger R. Dual-energy CT in the detection of bone marrow edema in the sacroiliac joints: is there a case for axial spondyloarthritis? Radiology. 2019;290(1):165–6.
48. Issa G, Mulligan M. Dual energy CT can aid in the emergent differentiation of acute traumatic and pathologic fractures of the pelvis and long bones. Emerg Radiol. 2020;27(3):285–92.
49. Dimopoulos M, Terpos E, Comenzo RL, Tosi P, Beksac M, Sezer O, et al. International myeloma working group consensus statement and guidelines regarding the current role of imaging techniques in the diagnosis and monitoring of multiple myeloma. Leukemia. 2009;23:1545–56. https://doi.org/10.1038/leu.2009.89.
50. Hillengass J, Usmani S, Rajkumar SV, et al. International myeloma working group consensus recommendations on imaging in monoclonal plasma cell disorders. Lancet Oncol. 2019;20:e302–12.
51. Terpos E, Kleber M, Engelhardt M, et al. European Myeloma Network. European Myeloma Network guidelines for the management of multiple myeloma-related complications. Haematologica. 2015;100:1254–66.
52. Moreau P, SanMiguel J, Sonneveld P, et al. ESMO Guidelines. Committee Multiple myeloma: ESMO clinical practice guidelines for diagnosis, treatment and follow-up. Ann Oncol. 2017;28(suppl 4):iv52–61.
53. Dimopoulos MA, Hillengass J, Usmani S, Zamagni E, Lentzsch S, Davies FE, et al. Role of magnetic resonance imaging in the management of patients with multiple myeloma: a consensus statement. J Clin Oncol. 2015;33(6):657–64.
54. Kosmala A, Weng AM, Heidemeier A, Krauss B, Knop S, Bley TA, Petritsch B. Multiple myeloma and dual-energy CT:

diagnostic accuracy of virtual noncalcium technique for detection of bone marrow infiltration of the spine and pelvis. Radiology. 2018;286(1):205–13.
55. Gu R, Amlani A, Haberland U, Hodson D, Streetly M, Antonelli M, Dregely I, Goh V. Correlation between whole skeleton dual energy CT calcium-subtracted attenuation and bone marrow infiltration in multiple myeloma. Eur J Radiol. 2022;149:110223. https://doi.org/10.1016/j.ejrad.2022.110223.
56. Kosmala A, Weng AM, Krauss B, Knop S, Bley TA, Petritsch B. Dual-energy CT of the bone marrow in multiple myeloma: diagnostic accuracy for quantitative differentiation of infiltration patterns. Eur Radiol. 2018;28:5083–90.
57. Werner S, Krauss B, Horger M. Dual-energy CT-based bone marrow imaging in multiple myeloma: assessment of focal lesions in relation. Acad Radiol. 2022;29:245–54.
58. Fervers P, Celik E, Bratke G, et al. Radiotherapy response assessment of multiple myeloma: a dual-energy CT approach with virtual non-calcium images. Front Oncol. 2021;23(11): 734819. https://doi.org/10.3389/fonc.2021.734819.
59. Chae EJ, Song JW, Seo JB, Krauss B, Jang YM, Song KS. Clinical utility of dual-energy CT in the evaluation of solitary pulmonary nodules: initial experience. Radiology. 2008;249(2):671–81.
60. Agrawal MD, Pinho DF, Kulkarni NM, Hahn PF, Guimaraes AR, Sahani DV. Oncologic applications of dual-energy CT in the abdomen. RadioGraphics. 2014;34(3):589–612.
61. Marin D, Nelson RC, Samei E, et al. Hypervascular liver tumors: low tube voltage, high tube current multidetector CT during late hepatic arterial phase for detection–initial clinical experience. Radiology. 2009;251:771–9.
62. Joe E, Kim SH, Lee KB, et al. Feasibility and accuracy of dual-source dual-energy CT for noninvasive determination of hepatic iron accumulation. Radiology. 2012;262:126–35.
63. Johnson TRC, Krauß B, Sedlmair M, Grasruck M, Bruder H, Morhard D, et al. Material differentiation by dual energy CT: initial experience. Eur Radiol. 2007;17(6):1510–7.
64. Apfaltrer P, Meyer M, Meier C, Henzler T, Barraza JM, Dinter DJ, et al. Contrast-enhanced dual-energy CT of gastrointestinal stromal tumors: is iodine-related attenuation a potential indicator of tumor response? Invest Radiol. 2012;47(1):65–70.
65. Hagspiel KD, Flors L, Housseini AM, Phull A, Ali Ahmad E, Bozlar U, et al. Pulmonary blood volume imaging with dual-energy computed tomography: spectrum of findings. Clin Radiol. 2012;67(1):69–77.
66. Jiang T, Zhu AX, Sahani DV. Established and novel imaging biomarkers for assessing response to therapy in hepatocellular carcinoma. J Hepatol. 2013;58(1):169–77.
67. Sun C, Miao F, Wang X-M, et al. An initial qualitative study of dual-energy CT in the knee ligaments. Surg Radiol Anat. 2008;30:443–7.
68. Agrawal MD, Pinho DF, Kulkarni NM, et al. Oncologic applications of dual-energy CT in the abdomen. Radiographics. 2014;34:589–612.
69. Johnson TRC, Krauss B, Sedlmair M, et al. Material differentiation by dual energy CT: initial experience. Eur Radiol. 2007;17:1510–7.
70. Hagspiel KD, Flors L, Housseini AM, et al. Pulmonary blood volume imaging with dual-energy computed tomography: spectrum of findings. Clin Radiol. 2012;67:69–77.
71. Schulz B, Kuehling K, Kromen W. Automatic bone removal technique in whole-body dual-energy CT angiography: performance and image quality. AJR Am J Roentgenol. 2012;199:646–50.
72. Simonetti I, Verde F, Palumbo L, et al. Dual energy computed tomography evaluation of skeletal traumas. Eur J Radiol. 2021;134: 109456.
73. Meinel FG, Bischoff B, Zhang Q, Bamberg F, Reiser MF, Johnson TR. Metal artifact reduction by dual-energy computed tomography using energetic extrapolation: a systematically optimized protocol. Invest Radiol. 2012;47(7):406–14.
74. Bamberg F, Dierks A, Nikolaou K, Reiser MF, Becker CR, Johnson TR. Metal artifact reduction by dual energy computed tomography using monoenergetic extrapolation. Eur Radiol. 2011;21(7):1424–9.
75. Zhou C, Zhao YE, Luo S, et al. Monoenergetic imaging of dual-energy CT reduces artifacts from implanted metal orthopedic devices in patients with factures. Acad Radiol. 2011;18(10):1252–7.
76. Kovacs DG, Rechner LA, Appelt AL, Berthelsen AK, Costa JC, Friborg J, Persson GF, Bangsgaard JP, Specht L, Aznar MC. Metal artefact reduction for accurate tumour delineation in radiotherapy. Radiotherapy Oncol. 2018;126(3):479–86. https://doi.org/10.1016/j.radonc.2017.09.029.
77. Yu L, Li H, Mueller J, et al. Metal artifact reduction from reformatted projections for hip prostheses in multislice helical computed tomography: techniques and initial clinical results. Invest Radiol. 2009;44(11):691–6.
78. Han SC, Chung YE, Lee YH, Park KK, Kim MJ, Kim KW. Metal artifact reduction software used with abdominopelvic dual-energy CT of patients with metal hip prostheses: assessment of image quality and clinical feasibility. AJR. 2014;203(4):788–95.
79. Andersson KM, Nowik P, Persliden J, Thunberg P, Norrman E. Metal artefact reduction in CT imaging of hip prostheses: an evaluation of commercial techniques provided by four vendors. Br J Radiol. 2015;88(1052):20140473.
80. Wang F, Xue H, Yang X, et al. Reduction of metal artifacts from alloy hip prostheses in computer tomography. J Comput Assist Tomogr. 2014;38(6):828–33.
81. Huang JY, Kerns JR, Nute JL, et al. An evaluation of three commercially available metal artifact reduction methods for CT imaging. Phys Med Biol. 2015;60(3):1047–67.
82. Lee YH, Park KK, Song HT, Kim S, Suh JS. Metal artefact reduction in gemstone spectral imaging dual-energy CT with and without metal artefact reduction software. Eur Radiol. 2012;22(6):1331–40.
83. Andersson KM, Norrman E, Geijer H, et al. Visual grading evaluation of commercially available metal artefact reduction techniques in hip prosthesis computed tomography. Br J Radiol. 2016;89(1063):20150993.